BBA - Bioenergetics 1866 (2025) 149508

Contents lists available at ScienceDirect

BBA - Bioenergetics

journal homepage: www.elsevier.com/locate/bbabio

Insights into electron transfer and bifurcation of the *Synechocystis* sp. PCC6803 hydrogenase reductase module

Elisabeth Lettau [a,b,*,1], Christian Lorent [b,1], Jens Appel [c], Marko Boehm [c], Paul R.F. Cordero [a], Lars Lauterbach [a,**]

[a] RWTH Aachen University, iAMB — Institute of Applied Microbiology, Worringerweg 1, 52074 Aachen, Germany
[b] Technische Universität Berlin, Institute of Chemistry, Straße des 14. Juni 135, 10623 Berlin, Germany
[c] Universität Kassel, Molecular Plant Biology, Heinrich-Plett-Straße 40, 34132 Kassel, Germany

ARTICLE INFO

Keywords:
Synechocystis sp. PCC6803
NAD^+-reducing hydrogenase
Reductase module
HoxEFU
HoxE
Iron-sulfur protein
Ferredoxin
Electron paramagnetic resonance (EPR)
Enzyme kinetics
Structure predictions

ABSTRACT

The NAD^+-reducing soluble [NiFe] hydrogenase (SH) is the key enzyme for production and consumption of molecular hydrogen (H_2) in *Synechocystis* sp. PCC6803. In this study, we focused on the reductase module of the *Syn*SH and investigated the structural and functional aspects of its subunits, particularly the so far elusive role of HoxE. We demonstrated the importance of HoxE for enzyme functionality, suggesting a regulatory role in maintaining enzyme activity and electron supply. Spectroscopic analysis confirmed that HoxE and HoxF each contain one [2Fe2S] cluster with an almost identical electronic structure. Structure predictions, alongside experimental evidence for ferredoxin interactions, revealed a remarkable similarity between *Syn*SH and bifurcating hydrogenases, suggesting a related functional mechanism. Our study unveiled the subunit arrangement and cofactor composition essential for biological electron transfer. These findings enhance our understanding of NAD^+-reducing [NiFe] hydrogenases in terms of their physiological function and structural requirements for biotechnologically relevant modifications.

1. Introduction

H_2 is an energy source with great potential, envisaged to replace fossil fuels in the future. However, the predominant reliance of industrial H_2 production on fossil raw materials underscores the urgent need for sustainable solutions. In this context, the coupling of H_2 production from hydrogenases with photosynthetic biocatalysts allows a clean and emission-free alternative, as recently demonstrated for photosystem I hydrogenase fusion complexes under anaerobic conditions [1,2]. For achieving light-driven H_2 production, NAD(P)H-dependent soluble hydrogenases (SH, group 3d) represent a promising choice. While the typical bacterial SHs only interact with NAD(H) and are applied also in oxidative and reductive cofactor regeneration [3–5], the cyanobacterial bidirectional SHs can reversibly transfer electrons to both $NADP^+$ and ferredoxins (Fig. 1a, b) [6,7].

The core structure of these multimeric enzymes can be divided into the hydrogenase module (HoxHY) with the catalytic [NiFe] active site and the reductase module harboring the flavin-based NAD(P)(H) binding site. The two modules are linked by a chain of at least five iron-sulfur clusters. The reductase module comprises at least the subunits HoxU and HoxF, which carries the flavin responsible for $NAD(P)^+$-cycling. While some bacterial O_2-tolerant hydrogenases, especially those with catalytic bias towards H_2 oxidation, contain additional two HoxI subunits, cyanobacterial hydrogenases incorporate another additional subunit (HoxE) in the reductase module (Fig. 1a) [8,9].

The physiological function of HoxE remains elusive. HoxE has a unique localization, being the sole subunit found in both the soluble and membrane fractions of cyanobacterial cells [9,10]. Therefore it was

Abbreviations: BSA, bovine serum albumin; CpI, *Clostridium pasteurianum* hydrogenase I; DT, sodium dithionite; EPR, electron paramagnetic resonance spectroscopy; FMN, flavin mononucleotide; ICP-OES, inductively coupled plasma optical emission spectroscopy; MBH, membrane bound hydrogenase; MV, methyl viologen; NAD(P)H, nicotinamide adenine dinucleotide (phosphate); NDH-1, NAD(P)H dehydrogenase complex; PFOR, pyruvate:ferredoxin oxidoreductase; RC I, respiratory complex I; RH, regulatory hydrogenase; SH, NAD^+-reducing hydrogenases, soluble hydrogenase.

* Corresponding author.
** Correspondence to: L. Lauterbach, RWTH Aachen University, iAMB — Institute of Applied Microbiology, Worringerweg 1, 52074 Aachen, Gemany.
E-mail addresses: elisabeth.lettau@rwth-aachen.de (E. Lettau), lars.lauterbach@rwth-aachen.de (L. Lauterbach).
[1] These authors contributed equally to this work.

https://doi.org/10.1016/j.bbabio.2024.149508
Received 12 May 2024; Received in revised form 3 September 2024; Accepted 4 September 2024
Available online 6 September 2024

proposed, that HoxE acts as a membrane anchor for the hydrogenase complex. Furthermore, deletion of HoxE *in vivo* results in a two- to threefold increase in the level of the remaining hydrogenase subunits, suggesting a potential regulatory function on the transcription level [11]. HoxE was also considered to be relevant for physiological electron transfer, since previous studies have shown that the presence of HoxE is essential for effective electron transfer between the redox couples $2H^+/H_2$ and NAD^+/NADH. Since HoxE carries a binding motif for a [2Fe2S] cluster, it was speculated that this subunit can also act as an electron acceptor for ferredoxins [12].

Compared to bacterial SHs, cyanobacterial hydrogenases have several binding motifs for additional iron-sulfur clusters (Supplementary Figs. S2 and S3), showing homologies to other metalloenzymes (Fig. 1c–e) [13]. Notably, the $[2Fe2S]^{E1}$ cluster in HoxE shares homologies with the N1a cluster in respiratory complex I (RC I) of *Thermus thermophilus*, as well as with the G7 cluster of formate dehydrogenase (FDH) from *Rhodobacter capsulatus* [14,15]. Furthermore, this binding motif is also found in the N-terminal region of HoxF, which is homologous to HoxE, presumably due to duplication [16]. The binding motif for an additional $[4Fe4S]^{U4}$ cluster in HoxU is homologous to that of the A1 cluster from *Rc*FDH, as well as to the proximal FS4A cluster of the monomeric [FeFe] hydrogenase from *Clostridium pasteurianum* (CpI) [14,17]. Previous studies investigated the iron-sulfur clusters of the cyanobacterial hydrogenase from *Synechocystis* by electron paramagnetic resonance (EPR) spectroscopy, where they identified signals for two different [2Fe2S] cluster and one [4Fe4S] cluster, although an assignment to specific iron-sulfur centers was not done [12,18]. Due to the high structural similarity of HoxU with the N-terminal part of FeFe-hydrogenases, which are known as ferredoxin oxidizing enzymes, the iron-sulfur clusters in HoxU were also suggested to be potential recipients of the electrons of ferredoxin [12,19]. Homologies to the possible additional iron-sulfur cluster $[2Fe2S]^{F2}$ in HoxF are also found in some of the HydABC hydrogenases, which are also able to interact with ferredoxins (Fig. 1f/g). These electron bifurcating enzymes interact simultaneously with NAD(P)H and reduced ferredoxin in an energy-conserving process to produce molecular hydrogen. Moreover, they show the highest sequence similarly to the *Syn*SH, apart from other cyanobacterial hydrogenases (Supplementary Table S2). Ferredoxin interaction in the HydABC hydrogenases is associated with the HydB subunit, which is homologous to HoxF [20–22].

Ferredoxin interaction is an important feature for coupling hydrogenases to photosystem I to achieve light-driven H_2 production in cyanobacteria under aerobic conditions [23]. Given that the interaction with ferredoxin is anticipated to take place at the reductase module, a thorough comprehension of the electron transfer and the associated iron-sulfur clusters is required. In this study, we aim to gain a comprehensive understanding of the functional role of HoxE, the interaction of the *Synechocystis* reductase module with ferredoxin, and the structure-function relationship of the iron-sulfur clusters involved. To achieve this, we engineered specific *Synechocystis* hydrogenase variants by selectively deleting individual subunits or iron-sulfur clusters. Using UV/Vis and EPR spectroscopy, we unambiguously identify the electronic structures of these clusters, providing valuable insights into the intricate workings of these versatile enzymes for the first time.

2. Methods

2.1. Plasmid construction

For heterologous overproduction of *Synechocystis* sp. PCC6803 HoxEFU derivatives in *Cupriavidus necator* HF903, all constructs were cloned into plasmid pCM66 [24]. All plasmids and primers used in this study are listed in Supplementary Table S1. Amplification of DNA fragments was performed using Phusion™ High Fidelity DNA Polymerase (New England Biolabs, Germany). Insertion of the *C. necator* SH promoter and a sequence encoding Strep-tag II was achieved by cloning of *Xba*I/*Bam*HI-treated pCM66 and pGE771 to form plasmid pLL71.3 [25]. Plasmid pLL9010.40 (Supplementary Fig. S1) was prepared by replacing bp 2458 to 4997 of pLL71.3 with a 3622 bp fragment of *Synechocystis* gDNA containing the *hoxEFU* genes using the assembly protocol described by Gibson [26] and primers 880fw/881rev and 882rev/883fw. Plasmid pLL9079 (Supplementary Fig. S1) was prepared by deletion of bp 2458 to 3055 harboring hoxE using primers 911fw/912rev. Insertion of a 576 bp fragment of *Synechocystis* sp. PCC6803 gDNA containing the *hoxE* gene with primers GB011/GB012 and GB009/GB010 into pLL9079 resulted in plasmid pEL37 (Supplementary

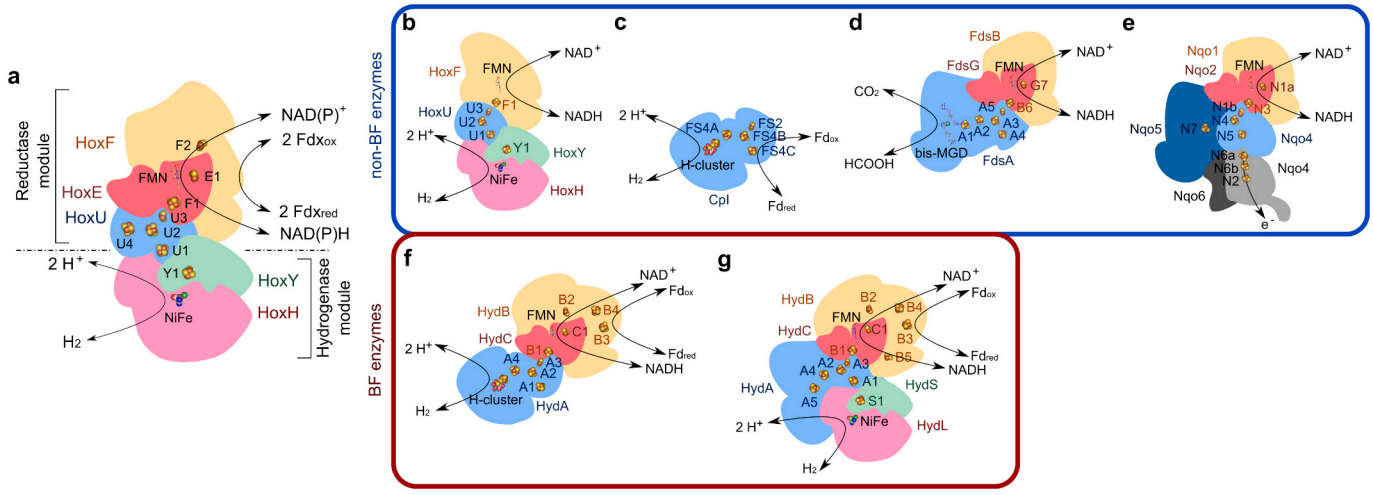

Fig. 1. Homologies of cyanobacterial $NAD(P)^+$-reducing hydrogenases to structures and cofactors of other metalloenzymes. a) Schematic representation of SH from *Synechocystis* sp. PCC6803 and comparison to structure and cofactor composition of homologue enzymes: b) bacterial SH from *Hydrogenophilus thermoluteolus* (PDB ID: 5XF9). Compared to the bacterial SHs, the cyanobacterial SHs have binding motifs for three additional iron-sulfur clusters (here: F2, E1 and U4) in the reductase module, homologies to these additional clusters can be found in c) monomeric [FeFe] hydrogenase from *Clostridium pasteurianum* (PDB ID: 1FEH), d) formate dehydrogenase from *Rhodobacter capsulatus* (PDB ID: 6TGA), e) cytoplasmatic domain of the respiratory complex I from *Thermus thermophilus* (PDB ID: 6Y11), f) trimeric HydABC [FeFe] hydrogenase from *Thermotoga maritima* (PDB ID: 7P5H) and g) HydABCSL [NiFe] hydrogenase from *Acetomicrobium mobile* (PDB ID: 7T30). The nomenclature of the iron-sulfur clusters is based on previous publications (if existent) and are numbered according to the subunit that harbors them. Non-electron bifurcating and electron bifurcating enzymes are grouped in blue (top) and red (bottom) boxes, respectively. (For interpretation of the references to color in this figure legend, the reader is referred to the web version of this article.)

Fig. S1). A ΔHoxU variant was generated by using primers Q5107F/Q5109R on plasmid pLL9010.40, for deletion of a 1445 bp fragment harboring an ORF and the *hoxU* gene, resulting in plasmid pEL05 (Supplementary Fig. S1). Plasmid pEL06 (Supplementary Fig. S1) was constructed using primers Q5107F/Q510R on plasmid pLL9010.40 for generation of the *Syn*HoxE only derivative. The deletion of the additional protentional [4Fe4S] cluster in HoxU was performed with either primer pair Q5103F/Q510xUR or Q5104F/Q510xUR on pLL9010.40, resulting in the plasmids pEL102 and pEL103, respectively (Supplementary Fig. S1). Plasmids were transferred by heat shock for selection in *E. coli* DH10β on Luria broth (LB) agar plates containing 50 μg mL^{-1} kanamycin. The correct cloning of the plasmids was verified by sequencing (Microsynth Seqlab, Göttingen, Germany) and then transferred by electroporation into the HoxFU-deficient *C. necator* strain HF903 (Δ*hoxG*, Δ*hoxB*, Δ*hoxFU*/MBH^-, RH^-, $HoxFU^-$).

2.2. Production and purification of reductase derivatives

For heterologous production of reductase derivatives, plasmids were transferred into *C. necator* by electroporation and selected on LB agar plates containing 200 μg mL^{-1} kanamycin. Minimal medium was used for protein production as described previously [27]. Precultures are grown in FN medium (fructose-ammonium) based on phosphate buffer (25 mM Na_2HPO_4 and 11 mM KH_2PO_4, pH 7.0) containing 0.4% (w/v) fructose, 0.2% (w/v) NH_4Cl, 0.81 mM $MgSO_4$, 0.068 mM $CaCl_2$, 18 μM $FeCl_3$, and 1 μM $NiCl_2$. Main cultures are grown in FGN (fructose-glycerol-ammonium) medium, which contains 0.05% (w/v) fructose and an additional 0.4% (w/v) glycerol, in contrast to FN medium. Precultures are grown at 37 °C overnight and main cultures are grown at 30 °C and 160 rpm for 7 days. Cell pellets are obtained by centrifugation at 6000 ×*g* for 30 min at 4 °C. Proteins were purified as previously described [28]. Pellets were resuspended in duplicate volume in argon-saturated resuspension buffer (50 mM Tris-HCl pH 8.0, 150 mM KCl, 5 % glycerol, 5 mM NAD^+, and cOmplete EDTA-free Protease Inhibitor Cocktail (Roche, Germany)). Cell disruption was performed by passing three times through a cooled French pressure cell (G. Heinemann) at 18,000 psi. The cell lysate was centrifuged at 36,000 rpm, 1 h, 4 °C (Beckman Coulter Optima XE-90 ultracentrifuge) and the supernatant transferred to a StrepTactin™ Superflow column (IBA, Göttingen, Germany) pre-equilibrated with basic buffer (50 mM Tris-HCl pH 8.0, 150 mM KCl, 5 % glycerol). Unbound protein was removed by washing twice with wash buffer I (50 mM Tris-HCl pH 8.0, 150 mM KCl, 5% glycerol, 5 mM NAD^+) and wash buffer II (50 mM Tris-HCl pH 8.0, 150 mM KCl, 5 % glycerol) sequentially. Purified enzyme was eluted in elution buffer (50 mM Tris-HCl pH 8.0, 150 mM KCl, 5% glycerol, 5 mM desthiobiotin) and concentrated in Amicon™ Ultra15 centrifugal filters with an appropriate exclusion size at 4000 ×*g* and 4 °C. Protein concentration was determined using the standard BCA protein assay, using bovine serum albumin as a standard (Pierce, Waltham, MA, USA). Success of protein production and purity was analyzed by SDS-PAGE (BioRad, MINI PROTEAN™ TGX Stain-FreeTM Gels) in TPE buffer (90 mM Tris, 10 mM EDTA, 2% (w/v) H_3PO_4 pH 7.6). The molecular mass of purified *Syn*-HoxEFU was determined by size exclusion chromatography (SEC) in filtrated potassium phosphate buffer (50 mM, pH 7.5) using a calibrated Superdex 200 column and defined size standards (thyroglobin 670 kDa, apoferritin 443 kDa, β-amylase 200 kDa, bovine serum albumin 66 kDa, carboanhydrase 29 kDa, hemoglobin 16 kDa, cytochrome C 12.3 kDa). The retention time was detected at 280 nm. *Synechocystis* PFOR (Sll0741) and Ferredoxin 1 (Ssl0020) were purified as described in Wang et al. and Artz et al., respectively [12,29].

2.3. Determination of cofactor saturation

The concentration of flavin mononucleotide (FMN) cofactor in reductase derivatives was determined photometrically in a plate reader (Infinite M Nano, TECAN) as described previously [6]. Duplicates of each protein samples (5 mg mL^{-1}) were denatured with an equal volume of 20% trichloroacetic acid (TCA) for 10 min at room temperature. After precipitation, the supernatant was neutralized with 20 μL of 1 M K_2HPO_4. The resulting solution was made up to a volume of 200 μL with millipore H_2O. FMN (Roth) was used to prepare standards. To determine the iron concentration of the reductase derivatives, metal analysis was performed using a PERKIN-ELMER Optima 2100DV inductively coupled plasma optical emission spectrometer (Perkin-Elmer, Fremont, CA, USA) according to the protocol described previously [28,30]. Briefly, protein samples were incubated with an equal volume of 65% nitric acid at 100 °C overnight. Samples were made up with 5 mL of water before ICP-OES analysis. As a negative control, buffer samples without protein were incubated in the same manner. Multielement standard solution XVI (Merck) was used as a reference.

2.4. Activity measurements

The NAD(P)H oxidation activity of the purified proteins was measured photometrically with an UV/Vis spectrophotometer (Varian Cary50 or Varian Cary60) by following the NAD(P)H-dependent reduction of artificial electron acceptors. Measurements were performed under anaerobic conditions in a 3-mL cuvette sealed with a rubber septum at 30 °C containing 1.9 mL of prewarmed and nitrogen-saturated assay buffer (50 mM potassium phosphate buffer pH 8.5). Immediately before the start of the measurement, 1 mM NAD(P)H and the respective redox dye were added to a final concentration of 5 mM benzyl viologen, 10 mM methyl viologen, 1 mM ferricyanide or 1 mM methylene blue. For measurements with benzyl viologen or methyl viologen, about 100 μM sodium dithionite was added to the reaction mixtures to remove any traces of oxygen. Reduction of benzyl viologen or methyl viologen was measured by following the absorbance increase at 578 nm (ε = 8.9 mM^{-1} cm^{-1} and 9.7 mM^{-1} cm^{-1}, respectively). Reduction of ferricyanide or methylene blue was measured by following the decrease in absorbance at 420 nm (ε = 1.02 mM^{-1} cm^{-1}) and 660 nm (ε = 71.5 mM^{-1} cm^{-1}), respectively. Reactions were started by adding 60.5 nM of the purified enzyme. For the determination of the reaction optima, the optimal temperature was first determined in the range of 5 to 70 °C and then the optimal pH was determined. A broad pH range CGT buffer (16 mM citric acid, 16 mM glycine, 16 mM 2-amino-2-(hydroxymethyl)propan-1,3-diol (Tris)) was used to determine the optimal pH. Different pH values between 5.5 and 10.0 were adjusted by titration with KOH. Each measurement was performed in triplicates. To measure ferredoxin-dependent NAD^+ reduction activity, a pyruvate ferredoxin reductase (PFOR) was used as a recycling system for reduced ferredoxin. For this purpose, the assay developed by Wang and co-workers was slightly modified [29]. Briefly, for a final volume of 1 mL, 4.5 mM ferredoxin was reduced for 30 min at room temperature (25 °C) in 100 mM Tris-HCl buffer pH 8.0 containing 270 μM PFOR, 0.5 mM coenzyme A, 10 mM pyruvate, 5 mM thiamine pyruvate phosphate as well as 40 mM glucose, 40 U glucose oxidase and 50 U catalase to induce anaerobiosis. The assay was started by adding 1 mM NAD^+ and 65 μM of the respective enzyme and the increase in absorbance at 340 nm (ε = 6.22 mM^{-1} cm^{-1}) was monitored spectrophotometrically. All samples were measured in triplicates.

2.5. Spectroscopic measurements

UV/visible spectra were recorded at 18 °C using a Varian Cary300 instrument. The final concentration of the protein samples was 1 mg ml^{-1} in 200 mM Tris-HCl buffer at pH 8.0 with 150 mM KCl and 5 % (w/v) glycerol. Reductase derivatives were reduced with a 50-fold excess of sodium dithionite under anaerobic conditions. Samples for electron paramagnetic resonance (EPR) spectroscopic experiments were prepared in the same buffer used for the UV/vis experiments. Aliquots (0.15–0.2 mM, 100 μL) of the respective protein solution were reduced under anaerobic conditions (100 % N_2) with a 50-fold excess of either

NADH or sodium dithionite. EPR spectra were recorded on a Brucker EMX plus X-Band spectrometer equipped with an ER 4122 super-high Q (SHQE) resonator and an Oxford ESR900 helium flow cryostat. An Oxford ITC4 temperature controller was utilized to adjust the temperature. The baseline correction was performed by subtracting a reference spectrum obtained from buffer solution recorded with identical experimental parameters. A polynomial or spline function was used to correct very broad baseline drifts. The experimental parameters used were: 1 mW microwave power, microwave frequency 9.29 GHz, modulation amplitude 10 G and 100 kHz modulation frequency. The MATLAB toolbox EasySpin version 5.2.36 was used for numerical simulating the EPR spectra, utilizing the core function pepper for calculating field-swept solid state EPR spectra [31].

2.6. In silico methods

The protein sequences used in this study were obtained from the UniProt data base. Multiple sequence alignments (MSAs) were performed using the Clustal Omega service of the EMBL's European Bioinformatics Institute (EMBL-EBI) [32]. Protein structures were obtained from the Protein Data Bank (PDB). In cases where experimentally determined structures were not available, protein structure models were calculated using the AlphaFold/AlphaFold 2.0 algorithm and evaluated using the pLDDT score [33–35]. The SWISS-MODEL service of the Swiss Institute of Bioinformatics (SIB) was used for prediction of quaternary protein structure assembly [36]. The model quality was assessed using the QMEANDisCo global score [36–38]. The AlphaFill algorithm facilitated the incorporation of ligands, cofactors and metals into the calculated structure models to generate holo-enzyme models [39]. The HDOCK server was used for protein-protein interaction modelling, with the credibility of the docking models assessed using the Confidence Score [40,41]. For the visualization of protein structures, the PyMOL software was used [42].

3. Results and discussion

3.1. Heterologous production of Synechocystis reductase derivatives for cofactor analysis

Different plasmids were constructed, harboring the respective genes for either the full *Synechocystis* reductase moiety HoxEFU or the subunit deletion mutants HoxFU, HoxEF, and HoxE. In addition, we constructed two different plasmids to delete the predicted additional [4Fe4S]^{U4} cluster in *Syn*HoxU (HoxEFU$^{\Delta U4a}$ and HoxEFU$^{\Delta U4b}$) (Supplementary Fig. S2). All constructs were under the control of the SH promoter from *C. necator*. For purification, a StrepTagII was fused to the N-terminal of either HoxE or HoxF. The plasmids were transformed into the reductase-deficient strain *C. necator* HF903 (Δ*hoxG*, Δ*hoxB*, Δ*hoxFU*/MBH$^-$, RH$^-$, HoxFU$^-$) for heterologous production.

The reductase derivatives were purified to homogeneity by one-step gravity flow affinity chromatography. No indications for co-purification of the *Cn*HoxHY were observed (Fig. 2a). From 10 g cell pellet (wet weight), an average of 4700 **µg** HoxEFU, 3960 **µg** HoxFU, and 410 **µg** HoxE was purified, sufficient for a comprehensive spectroscopic analysis. Size exclusion chromatography (SEC) on the isolated *Syn*HoxEFU derivative shows tetramerization of the complex (Supplementary Fig. S4). In contrast to similar proteins, the ΔHoxU derivative HoxEF and both Δ[4Fe4S]^{U4} variants HoxEFU$^{\Delta U4a}$ and HoxEFU$^{\Delta U4b}$ could only be purified in very low amounts and purity; these were, therefore, not further investigated (Supplementary Fig. S5) [43,44]. In addition, quantitative incorporation of the flavin mononucleotide cofactor (FMN) and the predicted iron-sulfur clusters was investigated by photometry and ICP-OES spectrometry, respectively. Based on sequence alignments, conserved binding motifs were predicted for four [4Fe4S] clusters and two [2Fe2S] clusters for the HoxFU derivative and an additional [2Fe2S] cluster for the HoxEFU derivative associated with the HoxE subunit

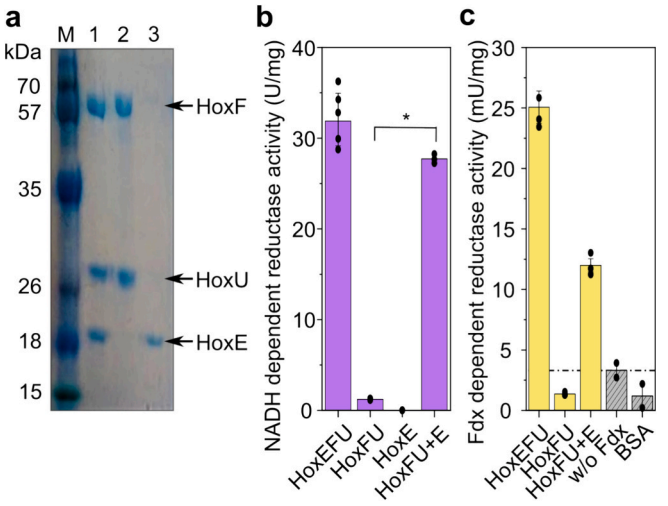

Fig. 2. Purification of functional reductase derivatives from *Synechocystis* sp. PCC6803 hydrogenase, which were heterologously produced in a reductase-deficient *C. necator* strain HF903. a) SDS PAGE of purified reductase derivatives HoxEFU (1), HoxFU (2), and HoxE (3); M-protein standard. Purified reductase derivatives show activity in b) NADH dependent reduction of methyl viologen and c) ferredoxin-dependent reduction of NAD^+. Error bars represent standard deviation of at least three individual replicates (dots), asterisk indicates a significant difference between HoxFU and HoxFU reconstituted with HoxE (p-value < 0.05). Dashed line indicates background activity, determined by negative controls without ferredoxin or with BSA instead of HoxEFU.

(Supplementary Figs. S2 and S3). Considering a respective maximum occupancy of 22, 20, or 2 iron atoms, an overall iron saturation of 13.5 iron atoms was determined for HoxEFU, 6 iron atoms for HoxFU, and 0.8 iron atoms for HoxE. The FMN content was calculated to be between 0.63 per HoxEFU and 0.7 per HoxFU molecule (Supplementary Table S3). With a variation range of up to 20 %, it is noticeable that the respective cofactor saturation is dependent on the respective batch. In contrast to previous work, where almost theoretical iron-sulfur content has been detected by EPR quantification [12]. The substoichiometric cofactor loading determined here may originate from protein over-determination, due to use of colorimetric assay [45], incomplete cofactor incorporation during biosynthesis, or loss of flavin during purification [6,46]. Activity assays of purified reductase derivatives revealed varying activities with different redox dyes as artificial electron acceptors. Methyl viologen yielded the highest NADH reduction activity, while ferricyanide and benzyl viologen showed lower and non-reproducible activities (see supplemental information for details, Supplementary Fig. S6). *In vitro* reconstitution with FMN did not affect activity (Supplementary Fig. S6). Highest activity was identified at 45 °C and pH 8.5, but resulted in shortened life-time and higher heterogeneity (Supplementary Fig. S7). Therefore, the most suitable assay conditions were standardized at 35 °C and pH 8.0 for the subsequent kinetic studies.

3.2. Role of HoxE for oxidoreductase activity

The HoxEFU-mediated turnover rate for the NADH-dependent oxidoreductase activity was 52.6 s^{-1}. An affinity constant (K′) for NADH of 54.4 µM was determined, which is comparable to the previously reported K_M values for the isolated *Synechocystis* and *C. necator* reductase moieties [12,28]. The NADH saturation curve of HoxEFU did not follow classical Michaelis-Menten kinetics, but shows slightly hyperbolic behavior (Supplementary Fig. S8); and was therefore fitted as Hill kinetic. The Hill coefficient was calculated as n = 1.45, thus indicating a positive cooperativity for substrate binding, possibly across individual reductase modules. This agrees with previous studies [12]

and a homotetramer formation, as suggested by size exclusion chromatography (Supplementary Fig. S4). Under the same conditions, the HoxFU derivative only shows turnover rates of 1.73 s^{-1} and the calculated K′ of 92.2 μM for NADH is only slightly higher than that of HoxEFU. In addition, the HoxFU derivative exhibited a lag phase of around 20 min, which was not observed for the HoxEFU derivative. Since HoxE lacks an NADH binding site, no NADH-dependent oxidoreductase activity could be measured in this derivative (Fig. 2b). Remarkably, when the HoxFU derivative was reconstituted *in vitro* with the isolated HoxE derivative in an equimolar ratio, activity could be detected immediately after addition of HoxE. A turnover rate of 30.9 s^{-1} and a K′ value of 74.1 μM was calculated for the reconstituted HoxFU+E derivative (Fig. 2b, Supplementary Table S4). A slight, but not significant, increase in activity was achieved when HoxE was in excess (HoxFU:HoxE ratios 1:1.4 and 1:2.8) in comparison to the whole reductase derivative HoxEFU (Supplementary Fig. S9).

The exact binding site for ferredoxin and the site for electron transfer from ferredoxin to *Syn*SH are still unknown. Based on cross-linking data, Artz and co-workers proposed that ferredoxin binds mainly to HoxF and partly to HoxE, with electron transfer to the [2Fe2S] cluster in HoxE [12]. To test this theory, the ferredoxin-mediated NAD^+-reducing capacity of the reductase derivatives described here was monitored photometrically. A pyruvate ferredoxin reductase (PFOR) was used as a recycling system for reduced ferredoxin. An activity of 25.1 mU mg^{-1} was determined for the complete reductase module (Fig. 2c, Supplementary Table S5). Similar to NADH dependent activity, a drastic decrease in activity was observed for the ΔHoxE derivative HoxFU, even lower than the negative controls (no ferredoxin added or BSA instead of the reductase derivatives). This confirms the relevance of HoxE to ferredoxin-dependent NAD^+-reducing activity. In addition, in vitro reconstitution of the HoxFU derivative with the isolated HoxE subunit led to a significant resurgence in activity, reaching 12.0 mU mg^{-1} (Fig. 2c, Supplementary Table S5). This provides further support for the previous theory that HoxE is responsible for the interaction with ferredoxin [12].

A correlation between the presence of HoxE and the activity of *Syn*SH has already been shown in previous studies, particularly with regard to electron transfer between $2H^+/H_2$ and NAD^+/NADH [9,47]. In addition, we have shown that this subunit is also indispensable for the isolated NADH/ferredoxin-dependent oxidoreductase activity, since the ΔHoxE reductase derivative only showed basal activity. However, activity of the ΔHoxE reductase derivative could be instantly restored by in vitro reconstitution with isolated HoxE, despite the fact that HoxE and the associated [2Fe2S] cluster are of pathway from the FMN to the [NiFe] active site (see next sections). These findings are in line with previous observations, which have shown that HoxE dissociates easily from the apo-enzyme, not only during purification of *Syn*SH but also *in vivo*, and therefore does not appear to be permanently associated with *Syn*SH [11,18].

3.3. Spectroscopic investigations

The cofactors in the reductase derivatives were further characterized by UV/Vis and EPR spectroscopy. The UV/Vis spectra of as-isolated *Syn*HoxEFU and *Syn*HoxFU (Fig. 3) showed a broad shoulder at around 456 nm, which can be attributed to oxidized FMN. Additional shoulders at 327 nm and 417/456 nm are consistent with the presence of oxidized [2Fe2S] and [4Fe4S] clusters. The absorbance spectra are very similar to those of isolated *C. necator* HoxFU and other homologous reductase modules, suggesting a predictable similar cofactor composition, although *Syn*HoxEFU has additional [2Fe2S] and [4Fe4S] clusters [28,48]. The UV/Vis spectra of as-isolated HoxE (Fig. 3) displayed distinct signals at 339 nm, 425 nm and 464 nm, which are typical for a ferredoxin-like [2Fe2S] cluster and strongly support the predicted iron-sulfur cluster in HoxE [49].

The findings from UV/Vis spectroscopy were further complemented with EPR spectroscopy. We used numerical simulations of the overlapping EPR signals to identify the individual species (Fig. S10). The EPR

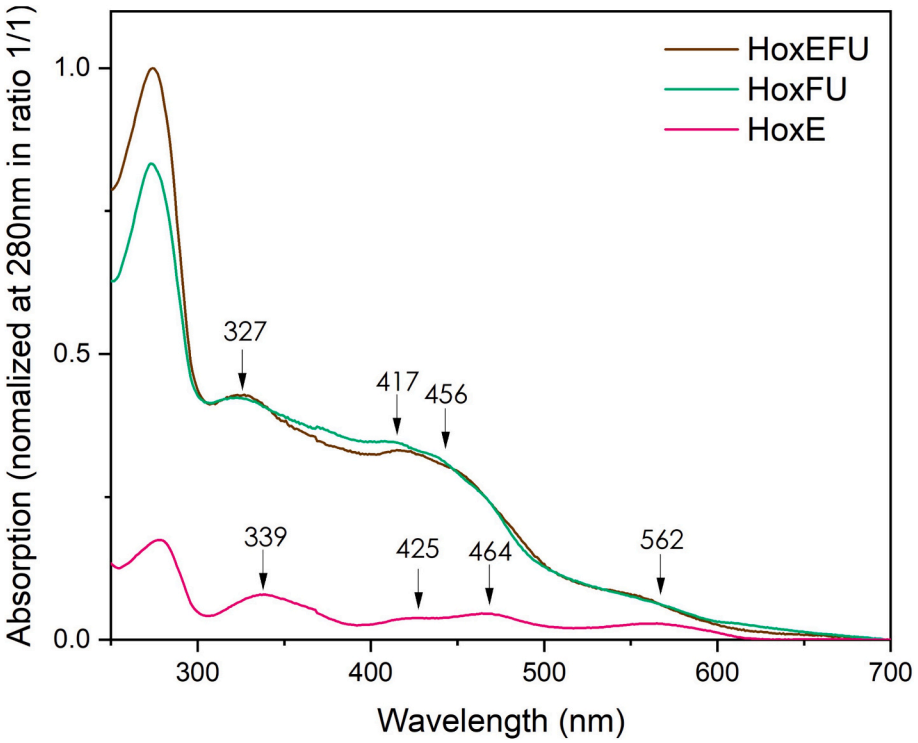

Fig. 3. UV/Vis spectra of the reductase derivatives *Syn*HoxEFU (brown line), *Syn*HoxFU (green line) and *Syn*HoxE (red line), each at a sample concentration of 1 mg mL^{-1}. The spectra are first normalized to the intense absorption band at 280 nm, which is related to the electronic transition of tyrosine and tryptophan and plotted in a molecular ratio of 1:1. (For interpretation of the references to color in this figure legend, the reader is referred to the web version of this article.)

spectrum of dithionite (DT)-reduced *Syn*HoxE recorded at 35 K (Fig. 4a, top) exhibits an intense rhombic signal ($g_x = 2.002$, $g_y = 1.945$, $g_z = 1.915$). Power saturation data of this species (Fig. 4c, Supplementary Table S6) indicates the characteristic behavior of a [2Fe2S] cluster without magnetic interactions to other paramagnetic centers in the vicinity [50]. The observed spectroscopic signature is almost identical to those of the homologous [2Fe2S] clusters (Supplementary Table S7) in *Escherichia coli*, *Paracoccus denitrificans*, and mammalian complex I, suggesting a highly conserved electronic structure of these metal sites [43,51,52]. The ΔHoxE derivative, *Syn*HoxFU, reduced by sodium dithionite (DT), showed two distinct EPR signals (Fig. 4a, middle) at 35 K. Based on the similarity to the characteristic spectral signatures of homologous [2Fe2S] clusters in RC I and other soluble [NiFe] hydrogenases (Supplementary Table 7), the axial species ($g_x = 2.017$, $g_y = 1.939$, $g_z = 1.929$) can be assigned to the [2Fe2S] cluster in HoxU, while the rhombic signal ($g_x = 2.001$, $g_y = 1.945$, $g_z = 1.915$) is likely related to the [2Fe2S] cluster in *Syn*HoxF. Notably, the latter signal is identical to the one of the [2Fe2S] cluster in HoxE in *Synechocystis*. This clearly elucidates why the EPR signals from those clusters could not be distinguished in the previous studies on the complete [NiFe] hydrogenase and HoxEFU reductase module from *Synechocystis* [12,18]. The power saturation of $[2Fe2S]^{F2}$ is clearly different compared to $[2Fe2S]^{E1}$ in isolated *Syn*HoxE (Fig. 4c, Supplementary Table S6). A weak dipolar interaction of $[2Fe2S]^{F2}$ with another paramagnetic center is suggested by a b-value below the limit for homogenous broadening ($b < 1$) [53]. As observed previously, additional broad signals attributed to the [4Fe4S] clusters appear at $g = 2.05$ and $g = 1.88$, when lowering the temperature to 10 K (Fig. 4d, e) [12,18]. Interestingly, the reduction by an excess of NADH only induced a minor enrichment of EPR active species (Fig. 4b, top), namely $[2Fe2S]^{U3}$ and a semiquinone radical ($g = 2.003$) from FMN. The signal from $[2Fe2S]^{U3}$ has a significantly different power saturation (Supplementary Fig. S11, Supplementary Table S6), exhibiting a much larger half-saturation power (5.93 mW vs. 0.01 mW), when reduced with DT instead of NADH. This indicates an accelerated spin relaxation rate, likely due to magnetic interactions with a paramagnetic site in proximity. Based on the structural proposal from Artz and coworkers [12] and our model (see below) this site is likely a [4Fe4S] cluster, suggesting that at least one of the two close-by [4Fe4S] clusters (F1 or U2) is reduced. Furthermore, the absence of a clear signal for $[2Fe2S]^{F2}$ at $g = 1.915$ (Fig. 4b, top) suggests, that this cluster cannot be reduced by NADH alone, possibly due to an impaired electron transfer from the FMN towards $[2Fe2S]^{F2}$ and/or a comparatively low reduction potential of this cluster (see below).

The EPR spectrum of the complete reductase complex (HoxEFU) reduced by DT (Fig. 4a, bottom) shows the same two EPR signals as in *Syn*HoxFU (Fig. 4a, middle). Merely the intensity of the rhombic [2Fe2S] cluster signal ($g_x = 2.001$, $g_y = 1.945$, $g_z = 1.915$) is much higher. Based on our previous interpretations, this species originates from the reduced $[2Fe2S]^{E1}$ and $[2Fe2S]^{F2}$ clusters. Notably, the calculated power saturation (Fig. 4c — pink trace, Supplementary Table S6) is very similar to $[2Fe2S]^{E1}$ in isolated *Syn*HoxE (Fig. 4c — red trace, Supplementary Table S6). This could indicate that there are no strong interactions between the two metal clusters inducing a clear relaxation enhancement or that the contribution from $[2Fe2S]^{F2}$ to this signal is rather minor. In contrast to *Syn*HoxFU, the signal from the reduced $[2Fe2S]^{U3}$ cluster is much more intense, while the semiquinone radical signal is diminished

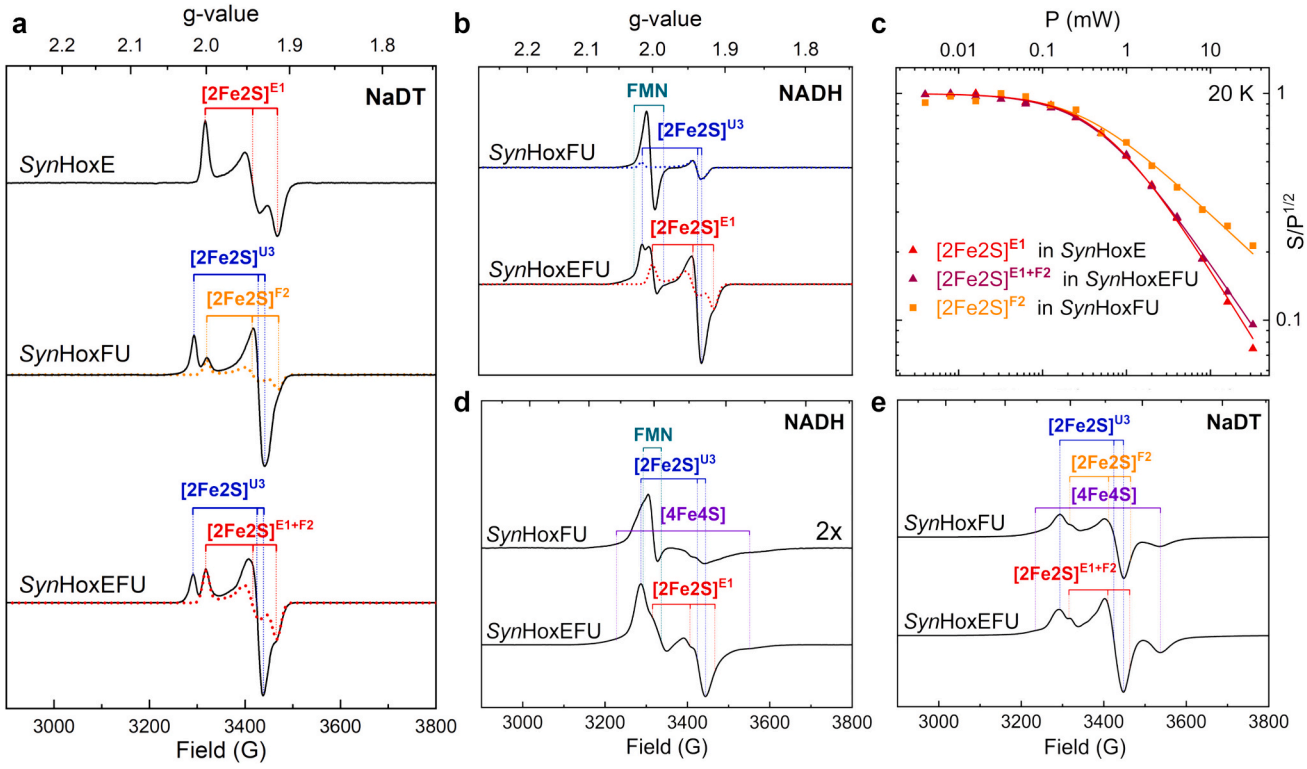

Fig. 4. Composition of HoxEFU derivatives analyzed by EPR spectroscopy (a) EPR spectra of *Syn*HoxE (top), *Syn*HoxFU (middle) and *Syn*HoxEFU (bottom) reduced with DT. (b) EPR spectra of *Syn*HoxFU (top) and *Syn*HoxEFU (bottom) reduced with NADH. The concentrations of the respective samples were 178 μM (HoxE), 211.5 μM (HoxFU) and 201.5 μM (HoxEFU), each in a volume of 100 μL. All spectra were recorded at 35 K. Signals assigned to the [2Fe2S] clusters are respectively labelled in red (E1), blue (U3), orange (F2), while those from flavin mononucleotide radicals are labelled in dark cyan. Simulated spectra of specific [2Fe2S] cluster signals are displayed as dotted lines. The corresponding simulations of all components and full spectra are presented in Supplementary Fig. S10. (c) Power saturation at 20 K of the [2Fe2S] cluster signal in DT-reduced E1 from *Syn*HoxE (red), E1 in *Syn*HoxEFU (pink) and F2 in *Syn*HoxFU (orange). Details of the power saturation are listed in Supplementary Table S6. (d) EPR spectra of NADH- and (b) DT-reduced *Syn*HoxFU and *Syn*HoxEFU both recorded at 10 K. Signals from [4Fe4S] cluster(s) (broad signals at $g = 2.05$ and $g = 1.88$) are labelled in purple. (For interpretation of the references to color in this figure legend, the reader is referred to the web version of this article.)

and even an additional rhombic [2Fe2S] cluster signal was observed in *Syn*HoxEFU when reduced by NADH (Fig. 4b). The larger number of reduced species in *Syn*HoxEFU coincides with the aforementioned enhanced NADH-dependent reductase activity, when the HoxE subunit is present. This underlines the vital role of HoxE for the NADH/NAD^+-dependent enzymatic reactivity as discussed also by Aubert-Jousset et al. [47] The additional EPR species is presumably related to $[2Fe2S]^{E1}$, since no signal from $[2Fe2S]^{F2}$ was observed in the NADH-reduced *Syn*HoxFU. Furthermore, $[2Fe2S]^{E1}$ is likely in electron transfer distance to the FMN (see next section) and could therefore directly accept electrons from NADH. However, the homologous N1a cluster of respiratory complexes I (RC I) usually cannot be reduced by NADH. An exception is the RC I of *E. coli*, for which spectral properties similar to those of *Syn*HoxEFU were reported along with an unusually high redox potential [51,53,54]. An important consideration in interpreting the EPR data is the difference in Fe content between *Syn*HoxEFU and *Syn*-HoxFU (13.5 of 22 vs. 6 of 20). The reduced Fe content in *Syn*HoxFU could lead to a disruption of the electron transfer pathway from FMN, particularly if an FeS cluster critical for this transfer is compromised. This disruption could result in the accumulation of the FMN semiquinone signal, as observed in the EPR spectra when NADH is used as the electron donor. Conversely, the presence of HoxE in *Syn*HoxEFU, with its higher Fe content, may maintain a more complete electron transfer chain, thereby reducing the intensity of the FMN semiquinone signal. Differences in the intensity of the EPR signals in the DT and NADH reduced samples may be due to different reduction potentials of NAD^+/NADH ($E^{0\prime} = -320$ mV) and DT ($E^{0\prime} = -660$ mV), but may also reflect the fact that reduction by NADH is dependent on activation at FMN and electron flow into the FeS chain, while DT can reduce the FeS clusters independently of reactivity with FMN. Thus, these differences may also affect the relative populations of reduced FeS clusters signals in the EPR experiments. The signals from [4Fe4S] cluster(s) were more pronounced in the EPR spectra at 10 K (Fig. 4d, e) from *Syn*HoxEFU compared to *Syn*HoxFU. This observation can be explained by the significantly lower iron content of the latter protein (see first section). Additionally, all EPR signals from electron-accepting groups are overall much less intense when reduced by NADH compared to DT (Fig. 4). This is in contrast to prior investigations, where NADH and DT both induced a similar level of reduction of the cofactors, but might again originate from an impaired electron distribution due to an incomplete cofactor occupancy. In particular, while DT can reduce the different cofactors directly, NADH is limited to FMN as access point to provide electrons and would therefore be more affected by an incomplete electron transport chain [12,18].

Putting all previous observations together and considering that *Syn*SH catalytically favours H_2 production [55], along its constitutive expression in *Synechocystis*, it is reasonable to infer that HoxE likely serves a regulatory function to avoid wasteful dissipation of redox equivalents [55–58]. This appears to be particularly important during dark fermentation, when *Syn*SH is neither inhibited by the oxygen produced by photosystem II nor in competition with ferredoxin-$NADP^+$ reductase (FNR) for reduced ferredoxin 1 (PetF) [59,60], especially since *Syn*SH has a much higher affinity for NADH than for NADPH, which are produced under dark fermentative and photosynthetically active conditions, respectively [7,12,47,61]. Taken together, this indicates a strong influence of HoxE on the activity and/or regulation of cyanobacterial hydrogenases, stemming from potential structural changes within the protein, stabilization of NAD^+/H binding, or a combination of both factors. Despite its close association with the HoxF subunit, which harbors the FMN and the NAD(P)$^+$/H binding sites, the $[2Fe2S]^{E1}$ does not appear to be part of the main iron-sulfur cluster chain. It is worth noting that, unlike homologous [2Fe2S] clusters, the $[2Fe2S]^{E1}$ can be reduced by NADH (Fig. 4a). This characteristic has only been uniquely identified in the N1a cluster of RC I from *E. coli*, whereas the same cluster in RC I from other species cannot be reduced by NADH due to its low redox potential [51,53]. The function of the N1a cluster has also remained a subject of debate. It was suggested to minimize production of reactive oxygen species (ROS), increasing the overall protein stability or inducing structural re-arrangements, that stabilize the NAD(H) binding [62–64]. Since, modulation of the redox potential of the respective cluster did not affect the (stoichiometry of) ROS production, it is unlikely that regulation occurs in this way [63]. Stabilization of the overall protein structure mediated by HoxE is rather unlikely, as stable, albeit inactive, subspecies of ΔHoxE-*Syn*SH can be observed in *Synechocystis in vivo* [65]. Moreover, we were able to isolate a stable ΔHoxE derivative of the *Synechocystis* reductase module. This leaves the induction of structural rearrangements and the stabilization of the NAD(H) binding as the most likely options. It remains unclear whether the $[2Fe2S]^{E1}$ cluster is needed for this purpose or if structural features of HoxE are decisive, since, related bacterial SHs lack this iron-sulfur cluster. Instead, the N-terminus of HoxF of these hydrogenases is extended and structurally homologous to HoxE.

3.4. Structural investigations reveal several potential ferredoxin interaction sites and similarity of SynSH with bifurcating hydrogenases

One of the most striking features of cyanobacterial SHs is their ability to use electrons from reduced ferredoxin to produce molecular hydrogen, though it is unclear where exactly ferredoxin binding takes place. To gain a better understanding of the structure of the *Synechocystis* reductase module, the positional relationship of the cofactors and potential interaction sites for ferredoxin, we calculated structural models of *Syn*HoxEFU/*Syn*SH using AlphaFold [33,34]. With a pLDDT value of over 87, the credibility of the calculated structure can be considered high. Subsequently, we fed this model of the apo-protein into the AlphaFill algorithm, which implements the ligands, cofactors, and metals from experimentally determined protein structures in order to generate a model of the holo-protein (Fig. 5, Supplementary Fig. S12) [39]. In addition to the high sequence identity of >47 %, a comparison of the calculated structure of *Syn*HoxEFU with experimentally solved structures of electron-bifurcating (BF) HydABC hydrogenases revealed a high structural identity. A comparison of the distances between the individual cofactors also showed that they differ by <1 Å (Supplementary Table S8). Since size exclusion chromatography revealed

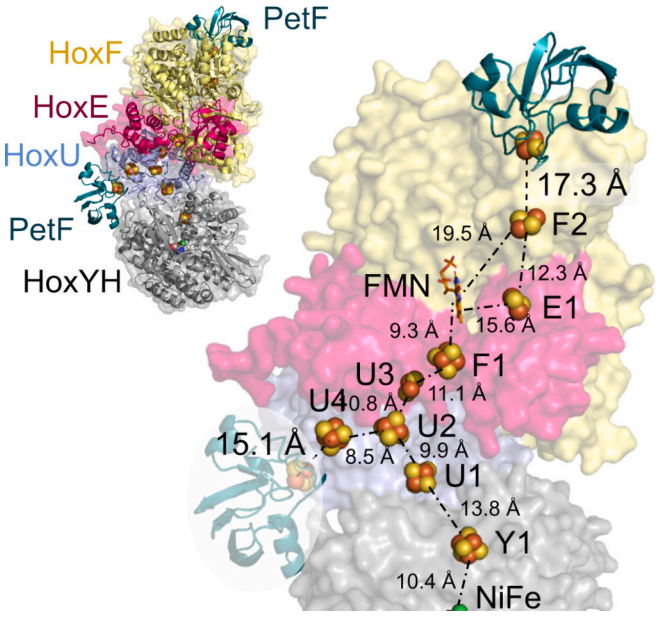

Fig. 5. AlphaFold structure of *Syn*SH, cofactors were inserted with the AlphaFill algorithm. Docking models calculated by HDOCK (Supplementary Fig. S13) reveal two potential binding sites for *Syn*PetF (cyan): one at HoxF and one at HoxU. (For interpretation of the references to color in this figure legend, the reader is referred to the web version of this article.)

tetramerization of the isolated reductase module, we built a homology model for *Syn*Hox(EFU)$_4$ based on *Tm*HydABC (PDB ID: 7P5H) using SWISSModel (Supplementary Fig. S12), QMEANDisCO global value was 0.7–0.05. According to this model, the [4Fe4S]^{U1} sites of two *Syn*HoxEFU units are in close proximity to each other (8.5 Å). This facilitates the exchange of electrons, which in turn explains the positive cooperation observed during kinetic characterization. It is notable that these two clusters are unlikely to be capable of electron exchange within the entire *Syn*SH enzyme, given that they are covered by HoxYH. Nevertheless, Eckert and co-workers put forth the hypothesis that *Syn*HoxEFU subpopulations also exist *in vivo* in *Synechocystis* [11].

Our structural model shows that the [2Fe2S]^{E1} cluster, as in RC I and *Rc*FDH, is located off-pathway to the [NiFe] center. However, unlike these two enzymes, it opens an additional electron pathway branch to the [2Fe2S]^{F2} cluster. Within the *Syn*HoxEFU molecule, the only electron transfer partner for [2Fe2S]^{F2} is the [2Fe2S]^{E1} cluster in HoxE, since a distance of 19.5 Å to the FMN is too large for efficient electron transfer. Furthermore, our calculated *Syn*HoxEFU structure reveals that the [2Fe2S]^{E1} cluster in HoxE is deeply buried in the protein scaffold. Only the [2Fe2S]^{F2} cluster in HoxF and the [4Fe4S]^{U4} cluster in HoxU are close enough to the surface (<5 Å) to receive electrons transferred by ferredoxins.

Docking predictions between our structure model of *Syn*HoxEFU and the *Synechocystis* ferredoxin (PetF) confirm these two potential binding sites at HoxF and HoxU, while no potential binding site was found at HoxE (Fig. 5, Supplementary Fig. S13; see supplemental material for details) [40,41,66]. The structural arrangement of the here presented PetF binding model is different from that proposed by Artz and co-workers [12], which was based on a homology model of *Ht*SH instead of the AlphaFold algorithm. Nevertheless, it underlines their findings based on cross-linking, showing evidence for PetF interacting mainly with HoxF. Since two electrons are necessary for production of molecular hydrogen, but PetF is only able to transfer one electron at a time, interaction with two PetF$_{red}$ one by one is mandatory. However, simultaneous interactions of two PetF at two different sites are also reasonable. The two predicted ferredoxin binding sites are accessible in the tetrameric structure model of *Syn*Hox(EFU)$_4$ (Supplementary Fig. S14). However, considering that native *Syn*SH can dimerize [9], the binding site on HoxU would be occupied (Supplementary Fig. S14), favoring the predicted binding site on HoxF. Nevertheless, the dimeric structure model is based on homology to SH from *Hydrogenophilus thermoluteolus* (*Ht*SH, PDB ID:5XF9), and there is no evidence to suggest whether *Syn*SH forms dimers in the same way as *Ht*SH or through other subunits, as proposed by Eckert et al. [11]

The fact that *Syn*SH is able to interact with both NAD(P)H and ferredoxin, and also shows high structural and sequential identity with electron bifurcating (BF) hydrogenases, raised the idea of a related functional mechanism. BF hydrogenases are specialized to couple exergonic and endergonic reactions, allowing the simultaneous H_2-driven reduction of NAD^+ and ferredoxin or vice versa (electron confurcation) [67]. Ferredoxin interaction of BF hydrogenases is proposed to take place at the HoxF homologue HydB subunit, particularly at the C-terminal domain that harbors two additional [4Fe4S] cluster, which are not present in HoxF (Fig. 1) [20–22,68,69]. Since these clusters are present in all described electron bifurcating hydrogenases, but not in the multimeric non-BF HydAB(C)-hydrogenases, they are believed to be essential for the bifurcation mechanism, by movement of the respective domain [20–22]. Furthermore, in the absence of structural data from *Syn*SH, there is no information available regarding the movement of domains within the reductase module. This contradicts the argument that *Syn*SH is an electron bifurcating hydrogenase. On the other hand, the non-BF HydAB(C) hydrogenases, unlike *Syn*SH, do not have the ability to interact with ferredoxin at all and all non-BF hydrogenases identified so far, also lack the binding motif for the additional [2Fe2S] cluster in the beta subunit (HoxF/HydB) [69].

Moreover, alignment of *Syn*HoxF with sequences of homologous subunits from known BF and non-BF enzymes revealed another structural feature that *Syn*SH shares with BF hydrogenases a signature motif in the shared FMN/NADH binding pocket, which is formed by a five-loop Rossmann-like fold. In 2020, Losey and co-workers discovered that in BF hydrogenases, three of these five loops contain typical motifs that are not conserved in non-BF hydrogenases: an alanine-phenylalanine-methionine (AFM) motif in the second loop, a phenylalanine (F) motif in the third loop, and a glycine-glycine-proline-serine-glycine (GGPSG) motif in the fourth loop [69]. All these signature motifs are completely conserved in *Syn*HoxF (Supplementary Fig. S15). The exact function of these conserved residues with respect to electron bifurcation can currently only be speculated, as few experimental structures and no mutagenesis studies on the corresponding amino acids are available. However, two observations can be made using structural models (Supplementary Fig. S15). First, the methionine in loop 2 is well positioned to affect the redox properties of [2Fe2S]^{E1}/FMN [70,71]. In addition, it may play a role in fine-tuning the redox potential of the [2Fe2S]. Second, phenylalanine in loop 3 may play a special role in coordination of the nucleotide cofactor, since tyrosine at this position in Nqo1 from *T. thermophilus* has been proposed to facilitate NADH binding through hydrogen bonding [62,65]. A comparison of the structures of known BF hydrogenases and non-BF enzymes also reveals that all non-BF enzymes lack the [2Fe2S] cluster, which is homologous to [2Fe2S]^{F2} of *Syn*HoxF (Supplementary Fig. S15). In conclusion, our structural predictions and comparisons shows a remarkable similarity between *Syn*HoxEFU and bifurcating hydrogenases. This supports the notion of a related functional mechanism, either in the form of a ferredoxin/NADH coupled reaction or even in a bifurcated mechanism. A bifurcating mechanism is characterized by a strict H_2:NADH:ferredoxin stoichiometry of 2:1:2 and would exclude the occurrence of half-reactions, as we could demonstrate by ferredoxin-dependent NAD^+ reduction with isolated *Syn*HoxEFU. However, it has also been shown in other bifurcating hydrogenases that thermodynamically favorable reactions are partially attainable in the absence of the third reaction partner, albeit with reduced conversion rates [72,73]. Nevertheless, activity measurements with the isolated *Syn*SH are necessary to clarify this. The low yields and the unequal ratios of individual subunits, in particular HoxE, after purification make it difficult to draw a conclusive interpretation [7,18]. Therefore, most activity assays with *Syn*SH have been performed in soluble cell extracts, which may still contain the complete components. While inactivity of purified *Syn*SH could also be due to sub-stoichiometric amounts of HoxE, it should be noted, that no activity of purified *Syn*SH has ever been demonstrated with ferredoxin alone, and in many cases, neither with NADH alone [7,18].

In a physiological context, *Syn*SH acts as an electron valve during the dark-light transition and produces H_2 [55,56]. The fact that H_2 production is short-lived has been explained by the oxygen sensitivity of *Syn*SH and competition for reduced ferredoxin with the FNR. However, it should also be considered that this is the only time when large amounts of cytosolic NADH and photosystem I-reduced PetF are simultaneously present in the cell, and efficient hydrogen production in this short phase could be accomplished by an electron bifurcation mechanism of *Syn*SH. Although *Syn*SH also produces small amounts of H_2 during dark fermentation, it is able to interact with other ferredoxins besides PetF that are reduced by other pathways [7,23]. Moreover, recent findings by Appel and co-workers showed electron transfer from *Syn*SH to photosynthetic complex I (NDH-1) [74]. Since H_2-dependent ferredoxin reduction is unfavorable, *Syn*SH is either reducing another electron mediator or it is directly interacting with the NDH-1 [56,74]. Another plausible explanation is electron bifurcation by the *Syn*SH, since this would allow H_2-dependent NAD^+/ferredoxin reduction, and the reduced ferredoxin could transfer electrons to NDH-1. Together, these findings improve our understanding of the *Synechocystis* bidirectional hydrogenase.

4. Conclusion

Our study provides significant insights into the structure of the reductase module of *Syn*SH and highlights the crucial role of the cyanobacterial SH-specific subunit HoxE for enzyme functionality. By demonstrating the presence of a [2Fe2S] cluster in the HoxE and HoxF subunits and identifying their spectroscopic fingerprints, we obtained a better impression of their roles in electron transfer. Furthermore, our predicted structural model of *Syn*HoxEFU elucidates the structural relationship of the subunits and cofactors with regard to their individual positions in the enzyme, emphasizing the structural identity shared with bifurcating hydrogenases. We propose that HoxE may have a regulatory function and optimizes electron supply. Our structure homology modelling and the observed interactions between *Syn*SH and ferredoxin facilitate the identification of possible ferredoxin binding sites at HoxF and perhaps at HoxU. The existence of signature motifs in *Syn*HoxF implies its involvement in electron bifurcation mechanisms. Collectively, our findings contribute to understanding the physiological role and relationships of *Syn*SH with other homologous enzymes. Future studies involving isolated *Syn*SH and improved purification techniques will be crucial for further investigating its activity and confirming its potential as a bifurcating hydrogenase.

CRediT authorship contribution statement

Elisabeth Lettau: Writing – review & editing, Writing – original draft, Visualization, Validation, Supervision, Methodology, Investigation, Formal analysis, Data curation, Conceptualization. **Christian Lorent:** Writing – review & editing, Writing – original draft, Visualization, Validation, Investigation, Formal analysis, Data curation. **Jens Appel:** Writing – review & editing, Resources. **Marko Boehm:** Resources. **Paul R.F. Cordero:** Writing – review & editing. **Lars Lauterbach:** Writing – review & editing, Supervision, Resources, Project administration.

Declaration of generative AI and AI-assisted technologies in the writing process

During the preparation of this work the author(s) used AlphFold 2.0 and AlphaFill in order to generate structural models of the enzyme. The author(s) used DeepL to improve readability and language of the manuscript. After using these tools/services, the author(s) reviewed and edited the content as needed and take(s) full responsibility for the content of the publication.

Declaration of competing interest

The authors declare that they have no known competing financial interests or personal relationships that could have appeared to influence the work reported in this paper.

Data availability

Data will be made available on request.

Acknowledgements

The authors acknowledge the support of the German Research Foundation (DFG grant no. 405325648, E.L. and L.L.). C. L. as part of the SPP 1927 within the project 311062227 (ZE 510/2-2). L.L. acknowledge the financial support from the Deutsche Forschungsgemeinschaft (DFG) under Germany's Excellence Strategy, EXC 2186 "The Fuel Science Center" ID:390919832, and Germany's Excellence Strategy EXC 2008 "UniSysCat" ID:390540038. We thank Oliver Lenz (Technische Universität Berlin) and Kirstin Gutekunst (Universität Kassel) for their generous support and helpful discussions as well as for providing lab space and equipment, Silke Leimkühler (Universität Potsdam) for metal analysis using ICP-OES. Nadine Brandt, Michelle Krause and Vanessa Franz for contributing during their research internship to this work.

Appendix A. Supplementary data

Supplementary data to this article can be found online at https://doi.org/10.1016/j.bbabio.2024.149508.

References

[1] J. Appel, V. Hueren, M. Boehm, K. Gutekunst, Cyanobacterial in vivo solar hydrogen production using a photosystem I–hydrogenase (PsaD-HoxYH) fusion complex, Nat. Energy 5 (2020) 458–467.
[2] A. Kanygin, et al., Rewiring photosynthesis: a photosystem I-hydrogenase chimera that makes H_2 in vivo, Energy Environ. Sci. 13 (2020) 2903–2914.
[3] A. Al-Shameri, et al., Synthesis of N-heterocycles from diamines via H_2-driven NADPH recycling in the presence of O_2, Green Chem. 21 (2019) 1396–1400.
[4] A. Al-Shameri, S.J.-P. Willot, C.E. Paul, F. Hollmann, L. Lauterbach, H_2 as a fuel for flavin- and H_2O_2-dependent biocatalytic reactions, Chem. Commun. 56 (2020) 9667–9670.
[5] A. Al-Shameri, D.L. Siebert, S. Sutiono, L. Lauterbach, V. Sieber, Hydrogenase-based oxidative biocatalysis without oxygen, Nat. Commun. 14 (2023) 2693.
[6] A.R. Weiss, H.G. Schlegel, Reduction of horse heart cytochrome c by the membrane-bound hydrogenase of *Alcaligenes eutrophus*, FEMS Microbiol. Lett. 8 (1980) 173–176.
[7] K. Gutekunst, et al., The bidirectional NiFe-hydrogenase in *Synechocystis* sp. PCC 6803 is reduced by flavodoxin and ferredoxin and is essential under mixotrophic, nitrate-limiting conditions, J. Biol. Chem. 289 (2014) 1930–1937.
[8] T. Burgdorf, et al., The soluble NAD^+-reducing [NiFe]-hydrogenase from *Ralstonia eutropha* H16 consists of six subunits and can be specifically activated by NADPH, J. Bacteriol. 187 (2005) 3122–3132.
[9] O. Schmitz, et al., HoxE—a subunit specific for the pentameric bidirectional hydrogenase complex (HoxEFUYH) of cyanobacteria, Biochim. Biophys. Acta Bioenerg. 1554 (2002) 66–74.
[10] N.J. Burroughs, et al., Solar powered biohydrogen production requires specific localization of the hydrogenase, Energy Environ. Sci. 7 (2014) 3791–3800.
[11] C. Eckert, et al., Genetic analysis of the Hox hydrogenase in the cyanobacterium *Synechocystis* sp. PCC6803 reveals subunit roles in association, assembly, maturation, and function, J. Biol. Chem. 287 (2012) 43502–43515.
[12] J.H. Artz, et al., The structure and reactivity of the HoxEFU complex from the cyanobacterium *Synechocystis* sp. PCC 6803, J. Biol. Chem. 295 (2020) 9445–9454.
[13] K. Zuchan, F. Baymann, C. Baffert, M. Brugna, W. Nitschke, The dyad of the Y-junction- and a flavin module unites diverse redox enzymes, BBA-Bioenergetics 1862 (2021) 148401.
[14] C. Radon, et al., Cryo-EM structures reveal intricate Fe-S cluster arrangement and charging in *Rhodobacter capsulatus* formate dehydrogenase, Nat. Commun. 11 (2020) 1912.
[15] J. Gutiérrez-Fernández, et al., Key role of quinone in the mechanism of respiratory complex I, Nat. Commun. 11 (2020) 4135.
[16] G. Boison, O. Schmitz, B. Schmitz, H. Bothe, Unusual gene arrangement of the bidirectional hydrogenase and functional analysis of its diaphorase subunit HoxU in respiration of the unicellular cyanobacterium *Anacystis nidulans*, Curr. Microbiol. 36 (1998) 253–258.
[17] M. Winkler, J. Esselborn, T. Happe, Molecular basis of [FeFe]-hydrogenase function: an insight into the complex interplay between protein and catalytic cofactor, BBA-Bioenergetics 1827 (2013) 974–985.
[18] F. Germer, et al., Overexpression, isolation, and spectroscopic characterization of the bidirectional [NiFe] hydrogenase from *Synechocystis* sp. PCC 6803, J. Biol. Chem. 284 (2009) 36462–36472.
[19] J.H. Artz, et al., Reduction potentials of [FeFe]-hydrogenase accessory iron–sulfur clusters provide insights into the energetics of proton reduction catalysis, JACS 139 (2017) 9544–9550.
[20] C. Furlan, et al., Structural insight on the mechanism of an electron-bifurcating [FeFe] hydrogenase, eLife 11 (2022) e79361.
[21] A. Katsyv, et al., Molecular basis of the electron bifurcation mechanism in the [FeFe]-hydrogenase complex HydABC, JACS 145 (2023) 5696–5709.
[22] X. Feng, G.J. Schut, D.K. Haja, M.W. Adams, H. Li, Structure and electron transfer pathways of an electron-bifurcating NiFe-hydrogenase, Sci. Adv. 8 (2022) eabm7546.
[23] S. Lupacchini, et al., Rewiring cyanobacterial photosynthesis by the implementation of an oxygen-tolerant hydrogenase, Metab. Eng. 68 (2021) 199–209.
[24] C.J. Marx, M.E. Lidstrom, Development of improved versatile broad-host-range vectors for use in methylotrophs and other Gram-negative bacteria, Microbiology 147 (2001) 2065–2075.
[25] L. Lauterbach, O. Lenz, Catalytic production of hydrogen peroxide and water by oxygen-tolerant [NiFe]-hydrogenase during H_2 cycling in the presence of O_2, J. Am. Chem. Soc. 135 (2013) 17897–17905.
[26] D.G. Gibson, Chapter fifteen — Enzymatic assembly of overlapping DNA fragments, in: C. Voigt (Ed.), Methods in Enzymology vol. 498, Academic Press, 2011, pp. 349–361.

[27] E. Schwartz, U. Gerischer, B. Friedrich, Transcriptional regulation of *Alcaligenes eutrophus* hydrogenase genes, J. Bacteriol. 180 (1998) 3197–3204.
[28] L. Lauterbach, Z. Idris, K.A. Vincent, O. Lenz, Catalytic properties of the isolated diaphorase fragment of the NAD^+-reducing [NiFe]-hydrogenase from *Ralstonia eutropha*, PLoS One 6 (2011) e25939.
[29] Y. Wang, et al., Pyruvate:ferredoxin oxidoreductase and low abundant ferredoxins support aerobic photomixotrophic growth in cyanobacteria, eLife 11 (2022) e71339.
[30] E. Lettau, et al., Catalytic and spectroscopic properties of the halotolerant soluble methane monooxygenase reductase from *Methylomonas methanica* MC09, ChemBioChem 23 (2022) e202100592.
[31] S. Stoll, A. Schweiger, EasySpin, a comprehensive software package for spectral simulation and analysis in EPR, J. Magn. Reson. 178 (2006) 42–55.
[32] F. Madeira, et al., Search and sequence analysis tools services from EMBL-EBI in 2022, Nucleic Acids Res. 50 (2022) W276–W279.
[33] J. Jumper, et al., Highly accurate protein structure prediction with AlphaFold, Nature 596 (2021) 583–589.
[34] R. Evans, et al., [Preprint] Protein complex prediction with AlphaFold-Multimer, biorxiv (2021), https://doi.org/10.1101/2021.10.04.463034.
[35] V. Mariani, M. Biasini, A. Barbato, T. Schwede, lDDT: a local superposition-free score for comparing protein structures and models using distance difference tests, Bioinformatics 29 (2013) 2722–2728.
[36] M. Bertoni, F. Kiefer, M. Biasini, L. Bordoli, T. Schwede, Modeling protein quaternary structure of homo- and hetero-oligomers beyond binary interactions by homology, Sci. Rep. 7 (2017) 10480.
[37] A. Waterhouse, et al., SWISS-MODEL: homology modelling of protein structures and complexes, Nucleic Acids Res. 46 (2018) W296–W303.
[38] G. Studer, et al., QMEANDisCo-distance constraints applied on model quality estimation, Bioinformatics 36 (2020) 1765–1771.
[39] M.L. Hekkelman, I. de Vries, R.P. Joosten, A. Perrakis, AlphaFill: enriching AlphaFold models with ligands and cofactors, Nat. Methods 20 (2023) 205–213.
[40] Y. Yan, H. Tao, J. He, S.-Y. Huang, The HDOCK server for integrated protein–protein docking, Nat. Protoc. 15 (2020) 1829–1852.
[41] S.-Y. Huang, X. Zou, An iterative knowledge-based scoring function for protein–protein recognition, Proteins Struct. Funct. Bioinf. 72 (2008) 557–579.
[42] W.L. DeLano, PyMOL: an open-source molecular graphics tool, CCP4 Newsl. Prot. Crystallogr. 40 (2002) 82–92.
[43] T. Yano, V.D. Sled, T. Ohnishi, T. Yagi, Expression and characterization of the flavoprotein subcomplex composed of 50-kDa (NQO1) and 25-kDa (NQO2) subunits of the proton-translocating NADH-quinone oxidoreductase of *Paracoccus denitrificans*, JBC 271 (1996) 5907–5913.
[44] T. Young, et al., Crystallographic and kinetic analyses of the FdsBG subcomplex of the cytosolic formate dehydrogenase FdsABG from *Cupriavidus necator*, J. Biol. Chem. 295 (2020) 6570–6585.
[45] S.P. Albracht, E. van der Linden, B.W. Faber, Quantitative amino acid analysis of bovine NADH: ubiquinone oxidoreductase (Complex I) and related enzymes. Consequences for the number of prosthetic groups, BBA-Bioenergetics 1557 (2003) 41–49.
[46] E. van der Linden, et al., Selective release and function of one of the two FMN groups in the cytoplasmic NAD^+-reducing [NiFe]-hydrogenase from *Ralstonia eutropha*, Eur. J. Biochem. 271 (2004) 801–808.
[47] E. Aubert-Jousset, M. Cano, G. Guedeney, P. Richaud, L. Cournac, Role of HoxE subunit in *Synechocystis* PCC6803 hydrogenase, FEBS J. 278 (2011) 4035–4043.
[48] K. Schneider, H.G. Schlegel, K. Jochim, Effect of nickel on activity and subunit composition of purified hydrogenase from *Nocardia opaca* 1b, Eur. J. Biochem. 138 (1984) 533–541.
[49] S.-C. Im, T. Kohzuma, W. McFarlane, J. Gaillard, A.G. Sykes, Formation, properties, and characterization of a fully reduced $Fe^{II}Fe^{II}$ form of spinach (and parsley)[2Fe-2S] ferredoxin with the macrocyclic complex $[Cr(15\text{-aneN4})(H_2O)_2]^{2+}$ as reductant, Inorg. Chem. 36 (1997) 1388–1396.
[50] W.R. Hagen, Biomolecular EPR Spectroscopy, CRC Press, 2009.
[51] M. Uhlmann, T. Friedrich, EPR signals assigned to Fe/S cluster N1c of the *Escherichia coli* NADH:ubiquinone oxidoreductase (complex I) derive from cluster N1a, Biochemistry 44 (2005) 1653–1658.
[52] T. Reda, C.D. Barker, J. Hirst, Reduction of the iron-sulfur clusters in mitochondrial NADH:ubiquinone oxidoreductase (complex I) by EuII-DTPA, a very low potential reductant, Biochemistry 47 (2008) 8885–8893.
[53] H. Leif, V.D. Sled, T. Ohnishi, H. Weiss, T. Friedrich, Isolation and characterization of the proton-translocating NADH: ubiquinone oxidoreductase from *Escherichia coli*, Eur. J. Biochem. 230 (1995) 538–548.
[54] Y. Zu, S. Di Bernardo, T. Yagi, J. Hirst, Redox properties of the [2Fe-2S] center in the 24 kDa (NQO2) subunit of NADH: ubiquinone oxidoreductase (complex I), Biochemistry 41 (2002) 10056–10069.
[55] C.L. McIntosh, F. Germer, R. Schulz, J. Appel, A.K. Jones, The [NiFe]-hydrogenase of the cyanobacterium *Synechocystis* sp. PCC 6803 works bidirectionally with a bias to H_2 production, J. Am. Chem. Soc. 133 (2011) 11308–11319.
[56] J. Appel, S. Phunpruch, K. Steinmüller, R. Schulz, The bidirectional hydrogenase of *Synechocystis* sp. PCC6803 works as an electron valve during photosynthesis, Arch. Microbiol. 173 (2000) 333–338.
[57] K. Gutekunst, et al., LexA regulates the bidirectional hydrogenase in the cyanobacterium *Synechocystis* sp. PCC 6803 as a transcription activator, Mol. Microbiol. 58 (2005) 810–823.
[58] E. De Rosa, et al., [NiFe]-hydrogenase is essential for cyanobacterium *Synechocystis* sp. PCC6803 aerobic growth in the dark, Sci. Rep. 5 (2015) 12424.
[59] L. Cournac, G. Guedeney, G. Peltier, P.M. Vignais, Sustained photoevolution of molecular hydrogen in a mutant of *Synechocystis* sp. strain PCC 6803 deficient in the type I NADPH-dehydrogenase complex, J. Bacteriol. 186 (2004) 1737–1746.
[60] Y. Sun, et al., Enhanced H_2 photoproduction by down-regulation of ferredoxin-$NADP^+$ reductase (FNR) in the green alga *Chlamydomonas reinhardtii*, Int. J. Hydrog. Energy 38 (2013) 16029–16037.
[61] O. Schmitz, et al., Molecular biological analysis of a bidirectional hydrogenase from cyanobacteria, Eur. J. Biochem. 233 (1995) 266–276.
[62] L.A. Sazanov, P. Hinchliffe, Structure of the hydrophilic domain of respiratory complex I from *Thermus thermophilus*, Science 311 (2006) 1430–1436.
[63] J.A. Birrell, K. Morina, H.R. Bridges, T. Friedrich, J. Hirst, Investigating the function of [2Fe2S] cluster N1a, the off-pathway cluster in complex I, by manipulating its reduction potential, Biochem. J. 456 (2013) 139–146.
[64] E. Gnandt, J. Schimpf, C. Harter, J. Hoeser, T. Friedrich, Reduction of the off-pathway iron-sulphur cluster N1a of *Escherichia coli* respiratory complex I restrains NAD^+ dissociation, Sci. Rep. 7 (2017) 8754.
[65] A.M. Burroughs, S. Balaji, L.M. Iyer, L. Aravind, A novel superfamily containing the β-grasp fold involved in binding diverse soluble ligands, Biol. Direct 2 (2007) 4.
[66] Y. Yan, D. Zhang, P. Zhou, B. Li, S.-Y. Huang, HDOCK: a web server for protein–protein and protein–DNA/RNA docking based on a hybrid strategy, Nucleic Acids Res. 45 (2017) W365–W373.
[67] J.W. Peters, A.-F. Miller, A.K. Jones, P.W. King, M.W. Adams, Electron bifurcation, COCHIBI 31 (2016) 146–152.
[68] N.A. Losey, F. Mus, J.W. Peters, H.M. Le, M.J. McInerney, *Syntrophomonas wolfei* uses an NADH-dependent, ferredoxinindependent [FeFe]-hydrogenase to reoxidize NADH, AEM 83 (2017) e01335–17.
[69] N.A. Losey, S. Poudel, E.S. Boyd, M.J. McInerney, The beta subunit of non-bifurcating NADH-dependent [FeFe]-hydrogenases differs from those of multimeric electron-bifurcating [FeFe]-hydrogenases, Front. Microbiol. 11 (2020) 1109.
[70] C.A. Gibbs, B.P. Fedoretz-Maxwell, G.A. MacNeil, C.J. Walsby, J.J. Warren, Proximal methionine amino acid residue affects the properties of redox-active tryptophan in an artificial model protein, ACS Omega 8 (2023) 19798–19806.
[71] V. Ramesh, K. Gibasiewicz, S. Lin, S.E. Bingham, A.N. Webber, Replacement of the methionine axial ligand to the primary electron acceptor A0 slows the A0-reoxidation dynamics in photosystem I, BBA-Bioenergetics 1767 (2007) 151–160.
[72] N. Chongdar, et al., Spectroscopic and biochemical insight into an electron-bifurcating [FeFe] hydrogenase, JBIC 25 (2020) 135–149.
[73] A. Kpebe, et al., An essential role of the reversible electron-bifurcating hydrogenase Hnd for ethanol oxidation in *Solidesulfovibrio fructosivorans*, Front. Microbiol. 14 (2023) 1139276.
[74] J. Appel, et al., Evidence for electron transfer from the bidirectional hydrogenase to the photosynthetic complex I (NDH-1) in the cyanobacterium *Synechocystis* sp. PCC 6803, Microorganisms 10 (2022) 1617.